Physics in Medicine & Biology

IPEM Institute of Physics and Engineering in Medicine

PAPER • OPEN ACCESS

Introducing the concept of spiral microbeam radiation therapy (spiralMRT)

To cite this article: Mattia Donzelli *et al* 2019 *Phys. Med. Biol.* **64** 065005

IOP Publishing Phys. Med. Biol. 64 (2019) 065005 (13pp) https://doi.org/10.1088/1361-6560/aaff23

Physics in Medicine & Biology

IPEM Institute of Physics and Engineering in Medicine

OPEN ACCESS

PAPER

Introducing the concept of spiral microbeam radiation therapy (spiralMRT)

Mattia Donzelli[1,2,3], Uwe Oelfke[2] and Elke Bräuer-Krisch[1,†]

[1] European Synchrotron Radiation Facility, Biomedical beamline ID17, Grenoble, France
[2] Joint Department of Physics at The Institute of Cancer Research and The Royal Marsden NHS Foundation Trust, London, United Kingdom
[3] Author to whom any correspondence should be addressed.
[†] Deceased on 10 September 2018.

E-mail: mail@donzelli.eu

Keywords: microbeam radiation therapy, spatial fractionation, spiralMRT, Monte Carlo simulation

RECEIVED
6 July 2018

REVISED
19 December 2018

ACCEPTED FOR PUBLICATION
16 January 2019

PUBLISHED
8 March 2019

Abstract

Motivation. With interlaced microbeam radiation therapy (MRT) a first kilovoltage radiotherapy (RT) concept combining spatially fractionated entrance beams and homogeneous dose distribution at the target exists. However, this technique suffers from its high sensitivity to positioning errors of the target relative to the radiation source.

With spiral microbeam radiation therapy (spiralMRT), this publication introduces a new irradiation geometry, offering similar spatial fractionation properties as interlaced MRT, while being less vulnerable to target positioning uncertainties.

Methods. The dose distributions achievable with spiralMRT in a simplified human head geometry were calculated with Monte Carlo simulations based on Geant4 and the dependence of the result on the microbeam pitch, total field size, and photon energy were analysed. A comparison with interlaced MRT and conventional megavoltage tomotherapy was carried out.

Results. SpiralMRT can deliver homogeneous dose distributions, while using spatially fractionated entrance beams. The valley dose of spiralMRT entrance beams is by up to 40% lower than the corresponding tomotherapy dose, thus indicating a better normal tissue sparing. The optimum photon energy is found to be around 150 keV to 200 keV.

Conclusions. SpiralMRT is a promising approach to delivering homogeneous dose distributions with spatially fractionated entrance beams, possibly decreasing normal tissue side effects in hypofractionated RT.

1. Introduction

Spatial fractionation is an approach in radiation therapy (RT) that uses highly inhomogeneous radiation fields which are periodically segmented into regions of high dose and regions of low dose separated by step-like gradients. The concentration of ionising radiation into confined volume sections, while not directly irradiating the remaining tissue, presents benefits for the recovery of normal tissue from radiation damage. This has been known since the beginning of the 20th century for grid therapy, where a coarse spatial fractionation with beam sizes in the order of millimetres to centimetres was used to spare the skin from high entrance doses (Laissue *et al* 2012) in orthovoltage RT.

Microbeam radiation therapy (MRT) (Bräuer-Krisch *et al* 2010) takes spatial fractionation to a much smaller scale, where arrays of parallel planar beams with sizes of tens to hundreds of micrometres are employed. The resulting dose pattern consists of dose peaks at the directly irradiated regions and dose valleys where only scattered particles can generate dose.

Microbeams with peak doses of hundreds of Gray have shown to inhibit tumour growth (Laissue *et al* 1998, Bouchet *et al* 2010, 2016), while healthy tissue exhibits an extraordinarily fast recovery after microbeam irradiation (Laissue *et al* 2001, Serduc *et al* 2006).

There is evidence that normal tissue tolerance to MRT mainly depends on the valley dose and that its dose thresholds for normal tissue complications correlate with the thresholds for conventional RT (Dilmanian *et al* 2002, Smyth *et al* 2016), as long as the width of the primary radiation peaks stays below a certain limit (Serduc *et al* 2014).

The disadvantage of orthovoltage x-rays used for MRT is the strong beam attenuation with depth demanding for a high entrance dose when treating deep-seated tumours. Amongst other techniques, interlacing microbeams (Dilmanian *et al* 2006, Serduc *et al* 2010) has been proposed to increase the dose to the tumour and reduce the dose at the beam entrance. The interlacing approach uses multiple microbeam arrays from different directions, where the microbeams from different arrays are aligned in parallel and neatly join with their edges.

The number of microbeam arrays, also called fields, from different directions can be increased such that the interlaced microbeams at the intersection completely fill up the target volume, generating a homogeneous dose distribution. The major advantage is a uniform high dose coverage of the target volume as in conventional radiation therapy, while the surrounding normal tissue benefits from spatial fractionation.

The challenge of interlaced microbeam irradiations is the required precision in positioning when changing the beam direction. The alignment between patient and radiation source requires a precision in the order of 10 μm. Otherwise, adjacent microbeams may overlap or leave gaps in the dose pattern. To date it is uncertain if this precision can be met with the currently available technology. Taking into account that the patient is deformable and moving adds another source of uncertainty, even if the positioning device meets the mechanical requirements.

As an alternative to interlaced microbeams, this publication presents the concept of spiral microbeam radiation therapy (spiralMRT)—a novel irradiation geometry which provides a homogeneous dose at the target and a spatial fractionation of the entrance beam, which can be delivered in one smooth and continuous movement of either the patient or the radiation source, thus avoiding the aforementioned potential errors in positioning.

2. The concept of spiral microbeam radiation therapy

The new irradiation geometry *spiral microbeam radiation therapy* (spiralMRT) uses a continuous irradiation with one single photon microbeam on a target which is performing a spiral motion, i.e. rotation and simultaneous translation along the rotation axis. As evident from figure 1, the microbeam cross section has its long extension along the tangential vector of the rotation and the short extension, which is responsible for the fluence modulation, parallel to the rotation axis. The centre of the microbeam is aligned with the rotation axis.

This setup results in a helical dose delivery, depositing a quasi-homogeneous dose inside a cylindrical volume centred on the rotation axis, where the pitch of the motion pattern is defined as the linear translation per one full rotation. The diameter and height of this cylinder of homogeneous dose naturally correspond to the horizontal extension of the primary microbeam and the range of the helical target motion during the irradiation. At the beam entrance, the microbeam structure is preserved by the rotation, resulting in a helical shape of the deposited dose.

There are several anticipated advantages of spiralMRT when compared to dose delivery with multiple static interlaced microbeam fields intersecting at the target:

- The overall beam entrance surface is increased, thus distributing the entrance dose over a larger volume and lowering it.
- The need for mechanical precision is reduced to continuous longitudinal and rotational motion, but there is no need for precise interlacing of several microbeam arrays. Positioning errors arising from mechanical backlash of the positioning device when moving source or patient up and down become irrelevant.
- Robustness to target motion is improved. In analogy to spiral computed tomography imaging, the continuous irradiation ensures that no part of the target can be missed due to organ motion between two irradiations from different directions.
- A short exposure time is usually demanded in MRT, in order to keep blurring of microbeams by organ motion as low as possible. This is achieved by using high dose rates around 10 kGy s^{-1} (Fournier *et al* 2016) produced at synchrotron sources. The exposure time at the target, where the dose distribution is homogeneous, is defined by the dose rate and the dose prescription. In the outer regions, the time span during which a tissue segment is actually exposed to the beam may be substantially shorter, which reduces the impact of microbeam blurring caused by organ motion.
  Furthermore, the homogeneous dose at the target will rather be in the order of 10 Gy–20 Gy, while pure microbeam treatments currently aim for doses bigger than 100 Gy in the microbeam peak. Thus, at equivalent dose rate, a shorter exposure time can be achieved.

The geometry was introduced here with a static radiation source and a moving target, but naturally the reversed setup consisting of a gantry-mounted rotating radiation source and a static target would equally work.

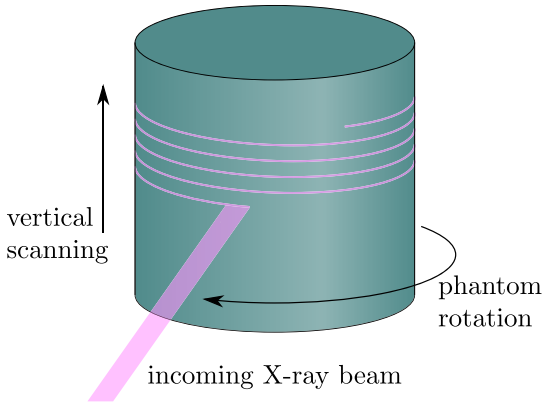

Figure 1. Illustration of the spiralMRT irradiation geometry. The target (green cylinder) performs a rotation and vertical translation while being continuously irradiated by a photon microbeam.

3. Method

The characteristics of a spiralMRT treatment are assessed using Monte Carlo methods for radiation transport. Variations of the photon energy, the microbeam pitch and the overall field size are taken into account in the simulations in order to identify their impact on the resulting dose distribution, which is assessed by extracting characteristic quality indicators. The details are explained in the sections here below.

3.1. Simulation and modelling

The achievable spiralMRT dose distributions are calculated in a simplified human head phantom, consisting of three different materials: skin, brain, and cortical bone according to the ICRU definition. The phantom is arranged in three coaxial cylinders of 175 mm height. The outer diameter is 175 mm with a 5 mm layer of skin and a 7 mm layer of bone, while the remaining inner part of the phantom is filled with brain material.

The calculation of dose deposition is carried out using a Monte Carlo simulation based on the Geant4 (Agostinelli *et al* 2003, Allison *et al* 2006) toolkit. As underlying physics model the Penelope physics list is employed.

The radiation source is modelled as a rectangular planar source emitting parallel monochromatic photons of homogeneous intensity perpendicular to its surface. In the calculations the source is moving on a spiral trajectory at 200 mm distance from the rotation axis around the static phantom in air. Rotation axis and cylinder axis of the phantom are chosen to coincide and the central axis of the incoming microbeam is perpendicular to the cylinder surface.

To facilitate the calculation, the reference system is chosen to have the phantom static and having the source rotate around it.

For modelling spiralMRT as a Monte Carlo simulation, the total irradiation time is calculated from the total field height and the linear component of the spiral motion in order to sample random points in time during the irradiation. From the random time point then the current position of the microbeam source can be calculated and a random position within the rectangular microbeam cross section is sampled to generate the origin of a photon.

The deposited dose is scored in a plane spanned by the cylinder axis of the phantom and an arbitrary radial vector of the corresponding cylinder. The scoring plane is segmented into 360 $\times$ 5000 pixels (along radial vector $\times$ along rotation axis) with a size of 500 μm $\times$ 5 μm, which results in a total extension of the scoring plane of 180 mm in lateral and 25 mm in vertical direction. The thickness of the scoring plane is 1 mm.

Within a range of 3 mm around the scoring plane, the tracking properties of the Monte Carlo simulation are adapted to the dimensions of the scoring grid. Secondary particle production cuts are reduced to 1 μm and the maximum step size for electrons is limited to 5 μm. Outside this fine tracking region, the simulation properties are coarser to improve the time-efficiency of the calculation.

The setup of the simulation geometry is shown in figure 2.

3.2. Selection of exemplary cases and parameters

A series of spiralMRT simulations was run with a fixed primary beam size of 50 μm $\times$ 20 mm and a total field height of the irradiated region of 20 mm. The field height is defined by the translation along the rotation axis of the helical motion.

A first set of spiralMRT data was acquired with three different beam energies (100 keV, 150 keV and 200 keV) at a pitch of 300 μm. For comparison a dose distribution of a 6-port interlaced microbeam geometry at 150 keV

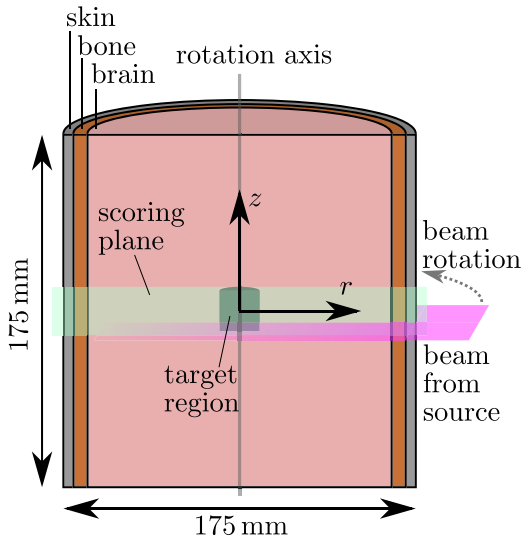

Figure 2. Transection view of the phantom geometry used for Monte Carlo simulations. The x-ray microbeam is entering from the right of the drawing and shown in pink. The drawing is not to scale.

photon energy was calculated. The interlaced microbeam irradiation consisted of six identical radiation fields, each composed of 67 beamlets (50 μm thick and 20 mm long) spaced by 300 μm pitch. The pitch is also known as centre-to-centre distance of the microbeam peaks. The beam angles were equally separated by 60°. It was made sure that microbeams from adjacent fields do not directly join.

Furthermore, an ideal monochromatic 2 MeV tomotherapy plan without intensity modulation and with homogeneous photon intensity was calculated, in order to compare spiralMRT to conventional RT. All configurations mentioned so far covered a total radiation field of 20 mm × 20 mm (horizontal extension × field height) at the target located in the centre of the phantom cylinder. The resulting cylindrical region of dose deposition in the phantom centre is also referred to as *target region*. The central beam axis is always perpendicular on the cylinder surface.

Based on the outcome of the first dataset, for 150 keV and 200 keV photon energy the pitch was increased to 450 μm and 600 μm in a second set of spiralMRT simulations. In the first simulation 100 keV photon energy did not appear as promising as 150 keV and 200 keV (see sections 4.1 and 4.3) and was therefore not included in the following simulations. Increasing the pitch is expected to result in a lower valley dose between the microbeams, which is associated with benefits for normal tissue (Dilmanian *et al* 2002, Smyth *et al* 2016). The field size was kept at 20 mm × 20 mm.

Finally, a comparison for field sizes of 20 mm × 20 mm, 10 mm × 10 mm and 2 mm × 2 mm at 150 keV spiralMRT and for a 2 MeV tomotherapy plan was generated to investigate the dependence of the outcome on the field size. The smallest field is of particular interest for applications in neurosurgery using ionising radiation, e.g. treatment of drug-resistant epilepsy (Romanelli *et al* 2012, Studer *et al* 2015, Pouyatos *et al* 2016).

All dose distributions were normalised to one at the centre of the target region, which is located at $r = 0$. To maintain comparability between the datasets and remove the impact of statistical noise, the dose distributions were divided by the average dose along the central 1.8 mm in z-direction, which correspond to the least common multiple of the different pitches used in this study.

The different parameter sets are summarised in table 1.

3.3. Analysis of the spatial fractionation properties

In order to evaluate the potential normal tissue sparing of orthovoltage spiralMRT, the calculated dose distributions are compared to megavoltage tomotherapy. As stated in section 1, the normal tissue sparing of spatially fractionated irradiation relies on the existence of an extended low-dose valley region. Thus, the spiralMRT valley dose must be lower than the tomotherapy dose to offer benefits to healthy tissue.

For all examined beam configurations, the central 1.8 mm of each dose distribution were analysed at different radii from the rotation axis. The volume fraction where the dose arising from spiralMRT irradiation is lower than the dose of the corresponding tomotherapy plan was extracted, alongside with the width of the regions where the peak dose is higher than the dose from tomotherapy. This is illustrated in figure 3. Furthermore, the mean dose in the region with a valley dose lower than the tomotherapy dose is calculated.

It should be noted that for the width of the peak a distinction between the higher entrance peaks and lower exit peaks must be made, as visible on figure 3. The exit peaks are due to the fact that the x-ray beam continues

Table 1. The different simulation configurations are grouped in 3 sets. The pitch is only relevant for spiralMRT and interlaced MRT.

Set 1—constant field size 20 mm × 20 mm—beam pitch 300 μm—variable photon energy	
Irradiation geometry	Photon energy
spiralMRT	100 keV, 150 keV, 200 keV
Interlaced	150 keV
Tomotherapy	2 MeV

Set 2—constant field size 20 mm × 20 mm—variable pitch—variable photon energy		
Irradiation geometry	Pitch	Photon energy
spiralMRT	450 μm	150 keV, 200 keV
	600 μm	150 keV, 200 keV
Tomotherapy	✗	2 MeV

Set 3—constant pitch 600 μm—constant photon energy—variable field size		
Irradiation geometry	Photon energy	Field size
spiralMRT	150 keV	$(2\ \text{mm})^2$, $(10\ \text{mm})^2$, $(20\ \text{mm})^2$
Tomotherapy	2 MeV	$(2\ \text{mm})^2$, $(10\ \text{mm})^2$, $(20\ \text{mm})^2$

propagating behind the target region. They appear in the middle of the valley regions between two entrance peaks due to the 180° offset of the propagation direction to the entrance peaks.

4. Results

The relative statistical uncertainties (1 standard deviation of the mean) of the dose distributions presented in this section are below 1% within the target region for all irradiation geometries. Outside the target region, the statistical uncertainties are below 1% for the entrance peaks (spiralMRT and interlaced MRT), below 4% for exit peaks and valley regions (spiralMRT and interlaced MRT), and below 3% for tomotherapy. For a better readability of the data, no error bars are plotted.

4.1. Dose distributions

The simulated doses showed the anticipated spatial pattern with a homogeneously irradiated region at the centre of rotation and a microbeam pattern along the beam in the outer regions. As shown in figure 4, the width of the dose peaks decreases with increasing radius from the rotation axis, due to the increasing cross-radial velocity of the phantom. The exposure time to the microbeam thus decreases and the impact of the smearing linear component of the spiral motion is reduced. More details on this aspect are given later on in section 5. The exit peaks appearing between each two entrance peaks can well be identified by their decreasing intensity with increasing radius, due to attenuation and decreasing exposure time as the angular velocity increases.

The detailed dose pattern in the vertical centre of the irradiated region ($z = 0$) is plotted in figures 5 and 6 for different radii. As expected, at $r = 0$ the dose profile is uniform for all cases. At the edge of the target region ($r = 10\,\text{mm}$) a ripple pattern is observed for spatially fractionated cases due to the slightly different penetration depth of the beam when impinging from different directions (see also figure 7, which depicts the dose fall-of with increasing penetration depth within the target region.). However, throughout almost the whole regarded region the dose is still higher than what would be delivered by tomotherapy without intensity modulation, which here only reaches ∼90% of the dose at the centre of the target.

Outside the homogeneously irradiated region, the dose pattern transforms into clearly separated microbeams. Figure 5 shows a distinctly higher valley dose for 100 keV photons, especially in the bone region around 80 mm radius, when compared to 150 keV and 200 keV photons.

Figure 6 shows that at large radius 200 keV photons give a lower minimum value in the valley than 150 keV photons, but also lead to more spreading of the microbeam peak due to the higher secondary electron range. This can be seen by the rounded edges at the interface between peak and valley region.

For a better understanding of the evolution of the dose deposited in the centre of the peak and the valley region with depth, these have been plotted in figure 7 according to the definition in figure 4. They show a clear reduction of the entrance peak dose and the valley dose outside the target region for photon energies of 150 keV and 200 keV compared to 100 keV. Photoelectric absorption of orthovoltage x-rays leads to increased doses in bone, in particular for low photon energies.

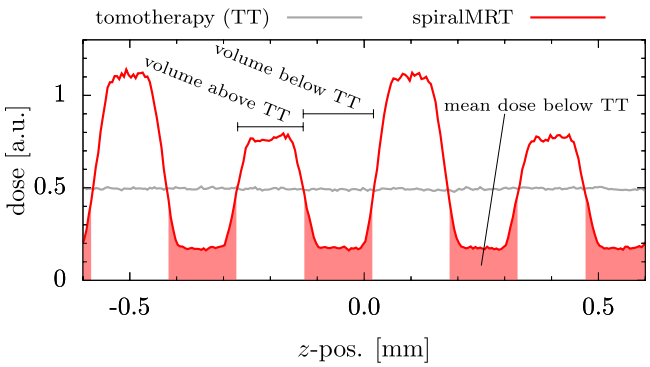

Figure 3. Definition of the characteristic values for the comparison of spiralMRT and tomotherapy. The regions indicated as *volume fraction below/above TT* are illustrating the volume where the spiralMRT dose is below/above the tomotherapy dose.

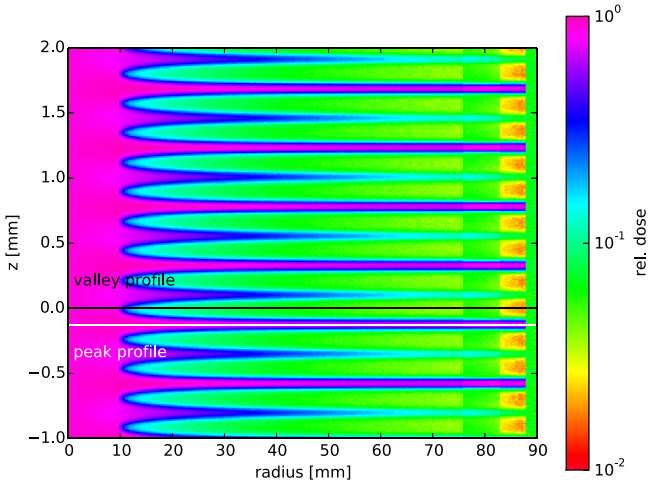

Figure 4. Dose distribution of the 200 keV/450 μm pitch dataset along the plane bisecting the phantom cylinder along its central axis. Note the different scales in the two dimensions and the logarithmic color bar. The indicated peak and valley profiles are plotted in figure 7 for different energies.

4.2. Dependence on the field size

Microbeam profiles at different radii are shown for different fields sizes in figure 8. All three presented cases exhibit a homogeneous dose close to the rotation axis. The 10 mm field provides a dose at the target border ($r = 5$ mm) which is higher than the dose from tomotherapy throughout the regarded volume.

As expected, assuming identical target dose, the peak and valley dose outside the target region are reduced when moving to smaller fields. However, in all cases the valley dose stays below the tomotherapy dose.

The 2 mm spiralMRT field in the right column exhibits a steep gradient and a box-like dose distribution. The tomotherapy dose distribution cannot provide such steep gradients and the dose distribution is less confined. This spiralMRT dose distribution is expected to be an advantage for the treatment of neurological indications like epilepsy, where small localised tissue portions are to be targeted.

4.3. Spatial fractionation properties

The characteristic values (mean dose below tomotherapy dose, volume fraction below tomotherapy dose, and width of the microbeams exceeding the tomotherapy dose) to compare spiralMRT and tomotherapy defined in section 3.3 are plotted in figure 9 for radii >10 mm. The data is separated into three columns which represent the three regarded pitches of 300 μm, 450 μm and 600 μm for spiralMRT and interlaced MRT in this study. The first two rows show the mean dose in the region that stays below the dose of a homogeneous 2 MeV tomotherapy irradiation, which is also plotted for comparison. The largest part of this region constitutes the valley region, but it includes also the lower part of the penumbra. The lower the dose is in this region is, the higher are the expected benefits for healthy tissue, as some authors (Dilmanian *et al* (2002) and Smyth *et al* (2016)) argue that MRT normal tissue tolerance depends on the valley dose and has similar threshold doses as conventional RT.

Subplots (a)–(c) show the dose normalised by the dose at the target point, while (d)–(f) show the same data normalised by the tomotherapy dose at the corresponding radius from the rotation axis. Subplot (d) shows data for 300 μm pitch and illustrates the aforementioned increase in valley dose for 100 keV photons at shallow depth.

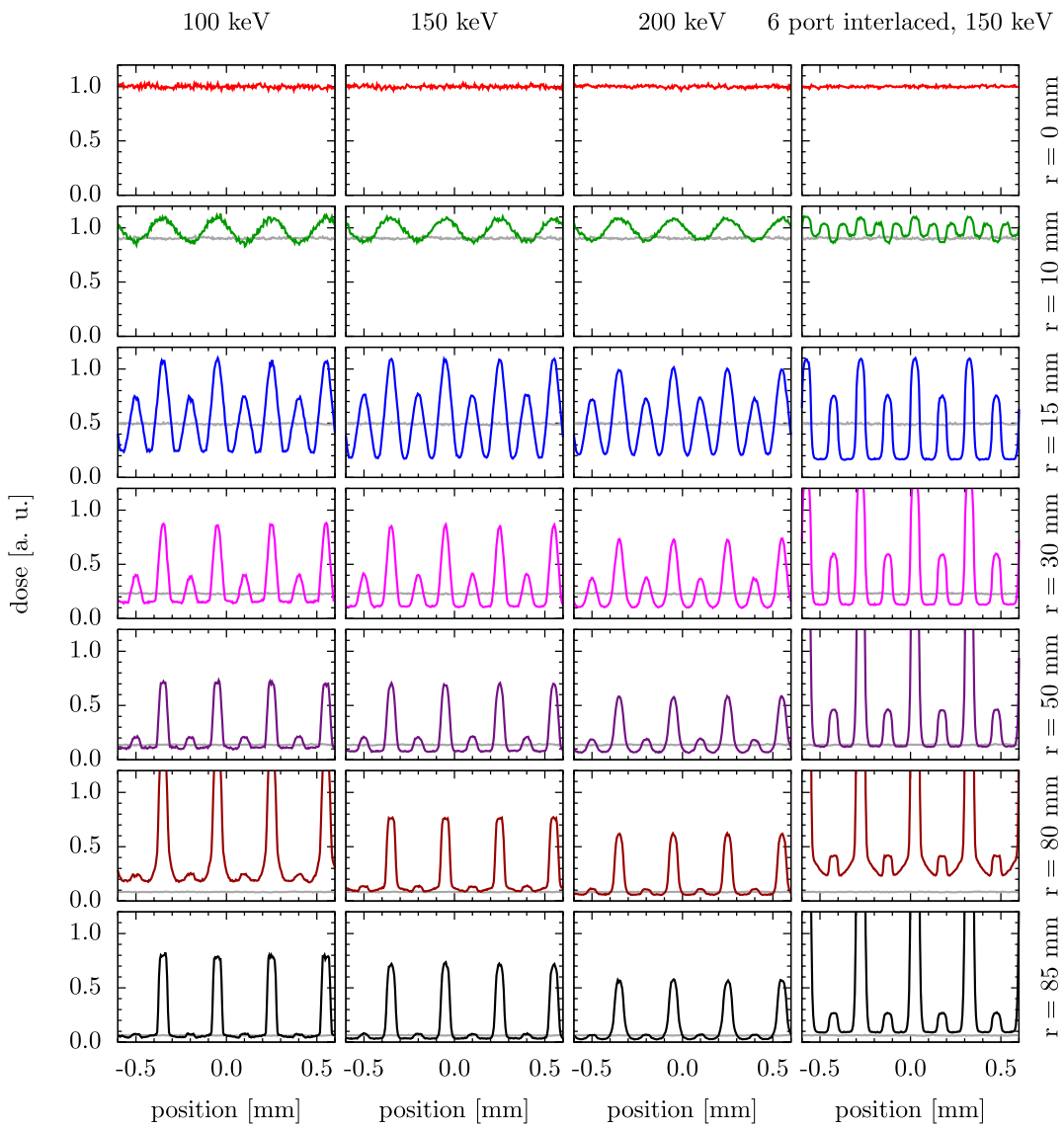

Figure 5. Dose profiles for different spatial fractionation schemes corresponding to set 1 in table 1 with 300 μm pitch and 20 × 20 mm^2 total field size. The first three columns show spiralMRT and the fourth column a 6-port interlaced geometry. At $r = 80$ mm the high absorption in the bone increases the dose. For comparison, the dose from the corresponding 2 MeV tomotherapy irradiation has been plotted as grey curve.

The 6-port interlaced geometry yields an extremely low dose close to the target, but then the normalised dose rises quickly towards the beam entrance. At $r > 60$ mm, peak and valley dose from interlaced MRT both stay above the reference dose from tomotherapy, therefore no data points for interlaced MRT are plotted above this radius in subplot (d).

Subplots (e) and (f) indicate that the valley dose can be lowered when increasing the pitch of the irradiation. With increasing radius, 200 keV achieve a lower dose in the regarded region than 150 keV photons, which is assumed to be advantageous. Where no data points are plotted (occurring in subplot (d) in the bone region), the valley dose entirely exceeds the tomotherapy dose at this radius.

The volume fraction that receives a lower dose than the reference tomotherapy dose is plotted in subplots (g)–(i). A large value is desired here, since it corresponds to a larger region where tissue damage is probably less severe than with tomotherapy. Here again, the 6-port interlaced geometry performs best in proximity of the target, but then rapidly declines. Increasing the spiralMRT pitch increases the volume fraction staying below the tomotherapy dose to some extend. Here, 150 keV photons produce slightly larger valley regions than 200 keV photons, except for the bone region.

The last row of subplots (j)–(l) scores the width of the region where the peak dose is above the tomotherapy dose. The entrance peaks (open symbols) for 150 keV photons are considerably smaller than for 200 keV. The energy-dependence for the exit beams (solid symbols) is less pronounced than for the entrance beams.

Furthermore, the beam pitch has a high impact on the peak width. While the minimum peak width is around 80 μm for 200 keV photons with 300 μm pitch, the minimum width at 600 μm pitch is in the order of 110 μm.

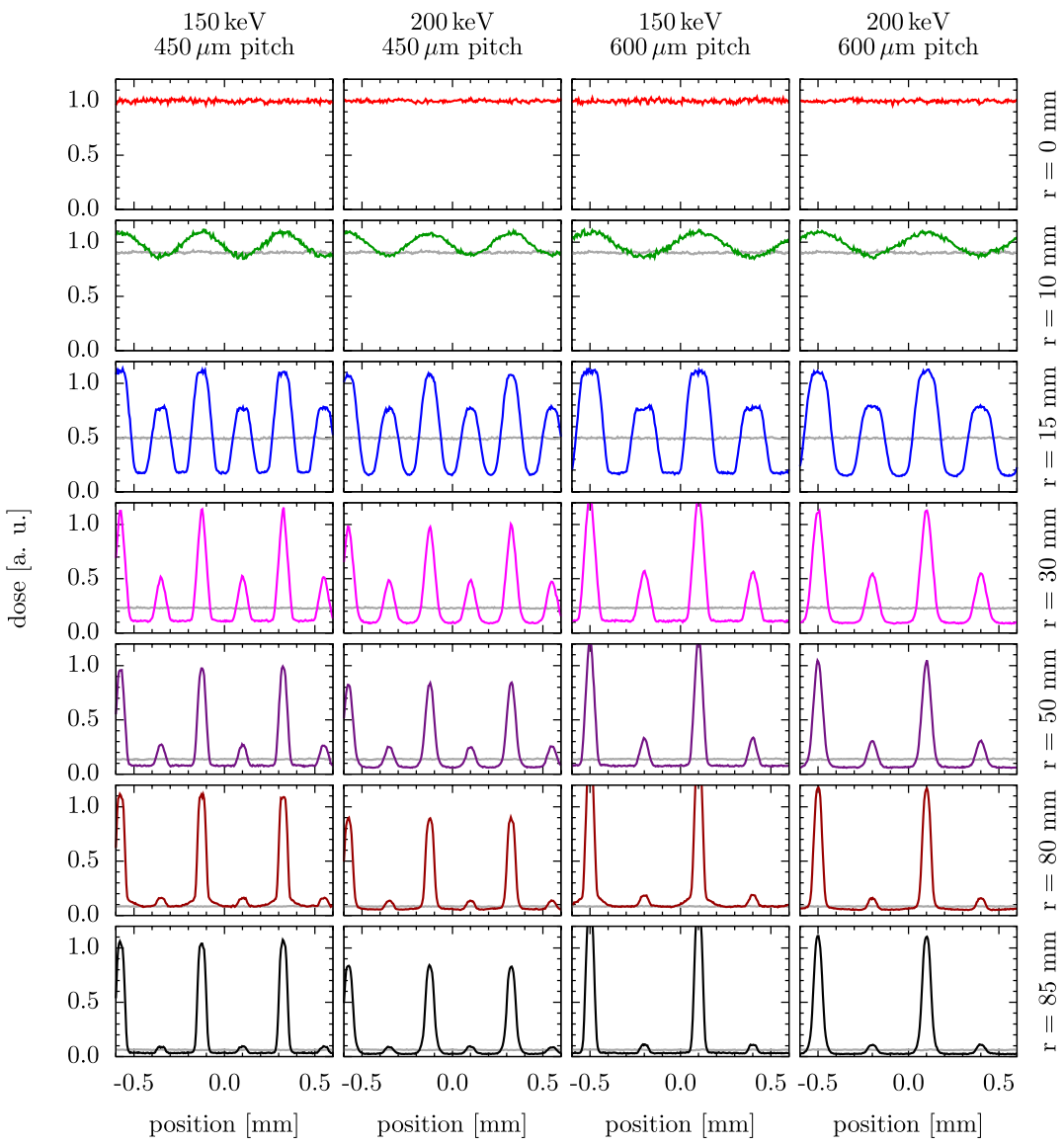

Figure 6. Dose profiles for spiralMRT with an increased pitch of 450 μm and 600 μm corresponding to set 2 in table 1. Tomotherapy shown in grey for comparison.

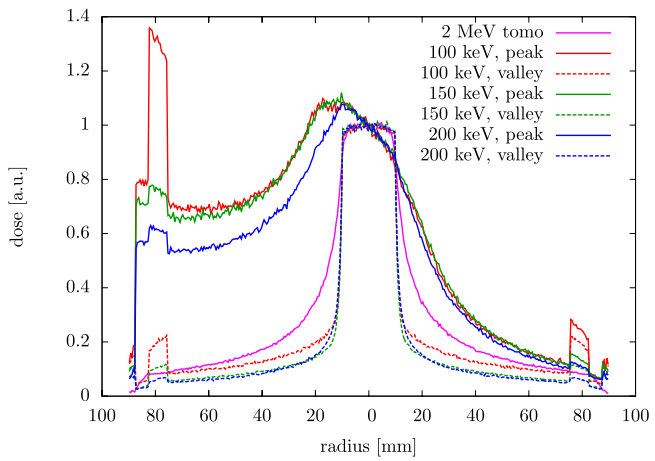

Figure 7. Radial dose profiles for 300 μm pitch spiralMRT at different energies and 2 MeV tomotherapy according to the definition in figure 4. The microbeam is entering from the left in this figure. Thus, the peak dose to the left of the target ($r = 0$) represents the entrance peak and to the right it represents the exit peak.

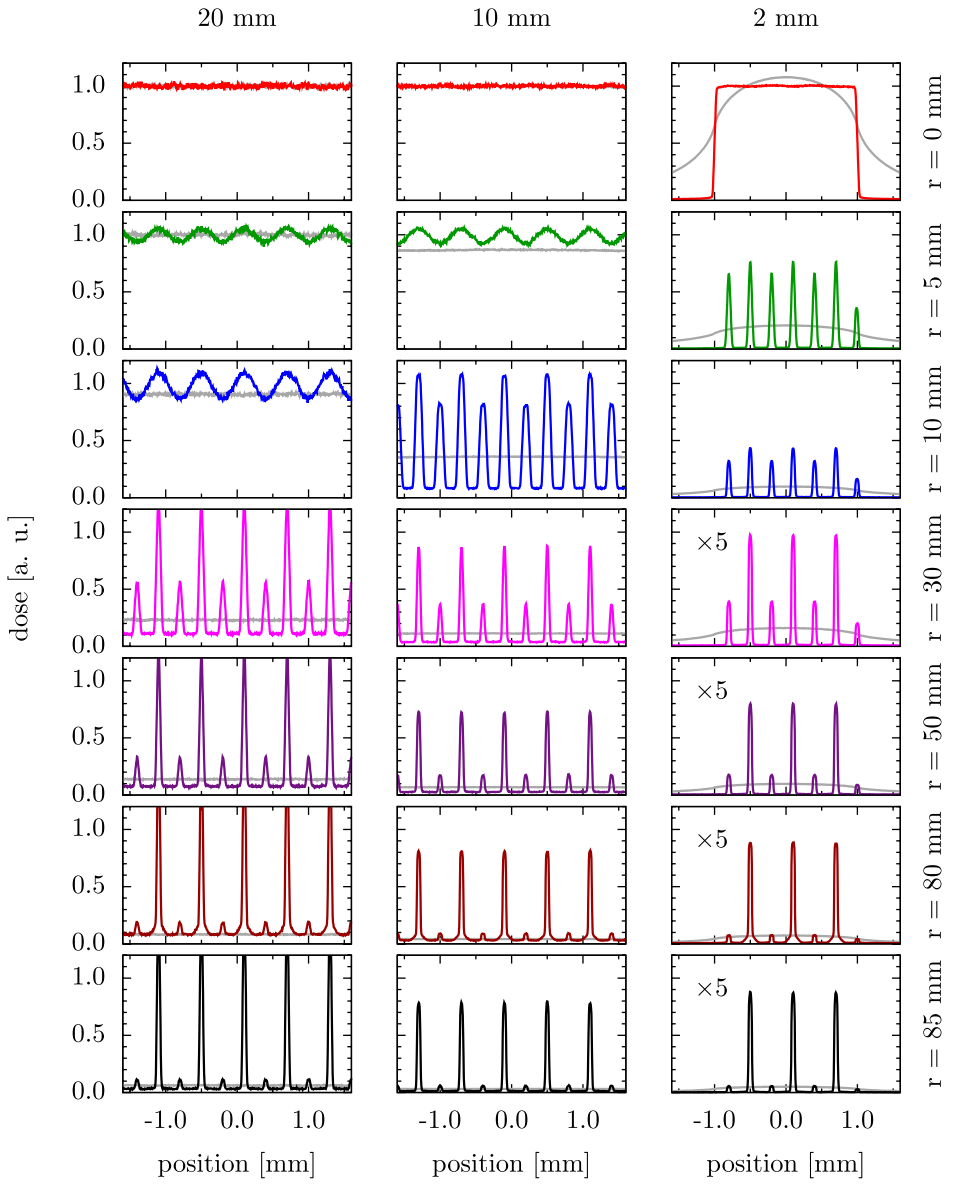

Figure 8. Dose profiles for spiralMRT for different fields sizes and a constant pitch of 600 μm corresponding to set 3 in table 1. In the third column the bottom four datasets have been scaled with a factor of five for better visibility. Tomotherapy shown in grey for comparison.

5. Estimation of the dose rates and exposure times

The rotation of the patient or the rotation of the source around the patient during irradiation has implications on the dose rates needed for a successful treatment. The faster the angular velocity is, the shorter the microbeam exposure time at the beam entrance becomes, which limits the effects of motion-induced blurring during irradiation. However, the dose rate, which is inversely proportional to the exposure time, needs to be increased accordingly.

The upper limit for patient rotation has been estimated to be 120° s^{-1} during synchrotron computed tomography imaging with humans (Renier 2016). An angular velocity of 90° s^{-1} is used there on a regular basis (Renier 2016).

The achievable target dose as a function of dose rate at reference conditions and the employed scan parameters were determined by comparison with the dose scored in a simulation of a 20 mm × 20 mm non-divergent radiation field impinging on a cubic 16^3 cm^3 water phantom in 20 mm depth from the phantom surface.

Using 200 keV photons and a hypothetical dose rate of 100 Gy s^{-1} at reference conditions and a linear component of the helical motion of 0.1 mm s^{-1}, the target dose would be 18.8 Gy and the revolution period 3 s, 4.5 s and 6 s for a pitch of 300 μm, 450 μm and 600 μm, respectively. 100 Gy s^{-1} is by a factor of 10–100 lower than the dose rates currently used in synchrotron-based MRT.

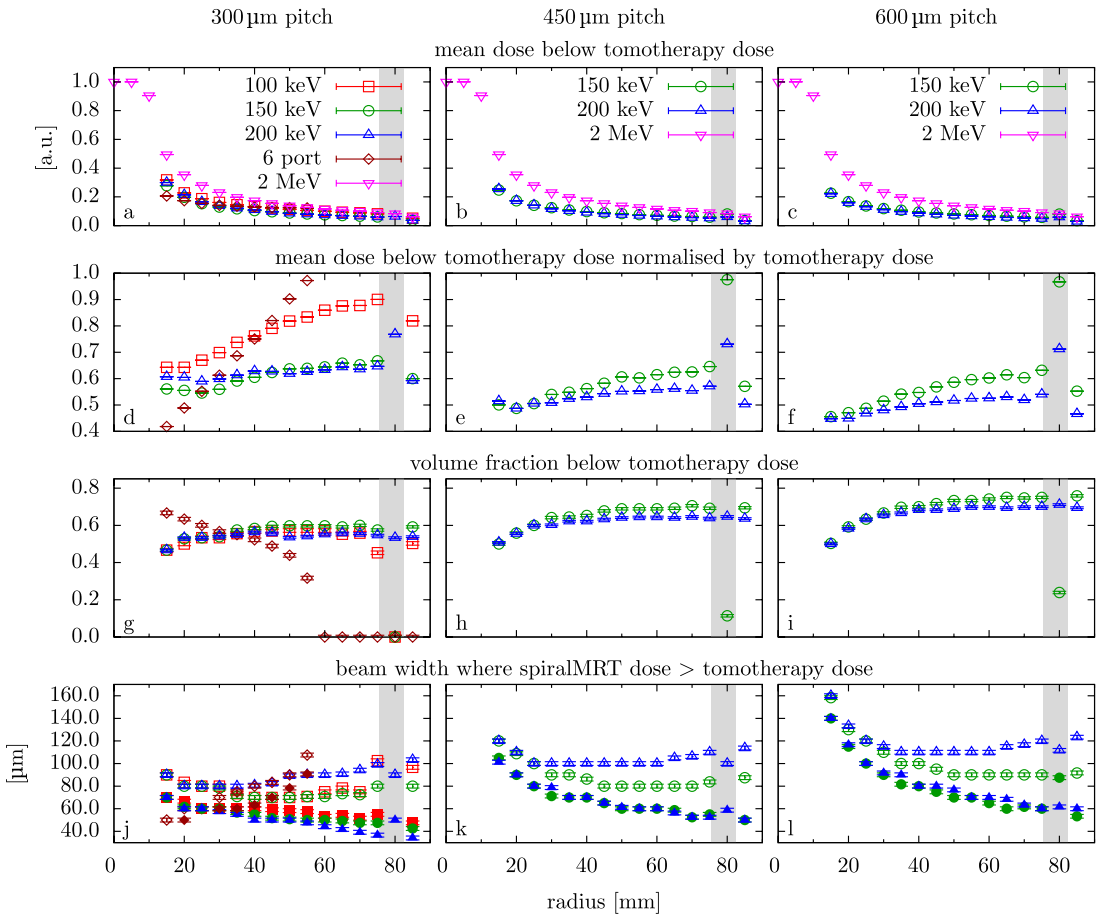

Figure 9. Compilation of different spatial fractionation properties of spiralMRT compared to the corresponding tomotherapy dose from sets 1 and 2 in dependence of the radius from the rotation axis. The grey shaded region represents the bone layer. All graphs share a common horizontal axis which is only labelled in the bottom line and represents the radius from the central rotation axis of the irradiation. The three columns represent datasets of equal pitch for the interlaced MRT and spiralMRT simulations (marked on top of each column). For each configuration, the tomotherapy dose for the same $20 \times 20\,\mathrm{mm}^2$ radiation field is plotted for comparison in the top row. The errorbars mark confidence intervals of one standard deviation. (a)–(c) The mean dose in the valley region that has a dose lower than the corresponding tomotherapy dose (marked as 2 MeV and plotted for comparison). (d)–(f) Same as the row above, but normalised by the tomotherapy dose at the same radius. (g)–(i) The volume fraction receiving a spiralMRT dose lower than the corresponding tomotherapy dose. (j)–(l) The width of the microbeams measured as the width of the regions having a dose higher than the corresponding tomotherapy dose. In these plots, open symbols represent the entrance beam, solid symbols the exit beam.

The required exposure time for this configuration is plotted as a function of the radius from the rotation axis in figure 10. In outer regions, where the tangential velocity is high, the exposure time is limited by the rotational movement and follows approximately an r^{-1} relationship. At smaller radius the exposure time is determined by the linear motion and independent of the radius.

In general, the exposure time is lowered by reducing the width of the field and by reducing the microbeam pitch at constant linear velocity.

6. Discussion

SpiralMRT presents an innovative approach in MRT with moderate entrance doses and could thereby reduce risks associated with peak doses in the hectogray region. At the same time it offers an opportunity to achieve a homogeneous high dose coverage of the target region, which is advantageous when comparing treatment outcome to conventional RT or when predicting tumour response. As mentioned in section 5, the demand for a high dose rate radiation source is much lower than in synchrotron based MRT with static beam directions.

In consistence with previous publications (Spiga *et al* 2007, Shinohara *et al* 2014) on MRT, 100 keV photons, which are closest to the spectrum currently used in MRT at the ESRF (Crosbie *et al* 2015) and the Australian Synchrotron (Livingstone *et al* 2016), are below the optimum energy for spiralMRT. 150 keV and 200 keV offer a better penetration due to reduced x-ray absorption. As a result, the valley doses are substantially lower than for 100 keV. Photon energies above 200 keV are assumed to have too large secondary particle ranges, which will lead to a larger microbeam penumbra and increased valley dose.

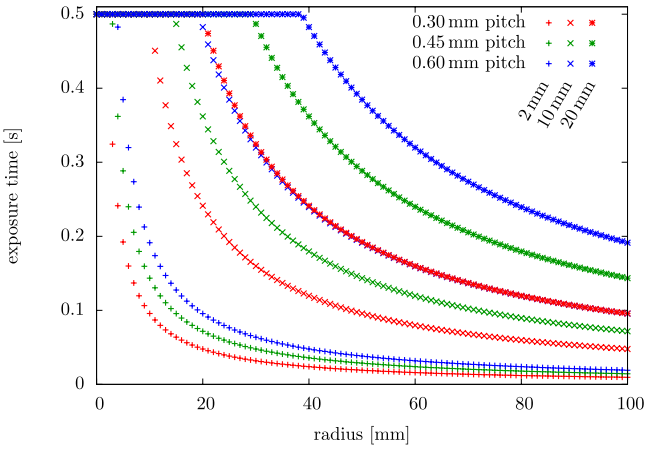

Figure 10. The exposure time during which the primary microbeam irradiates a certain point in space in dependence of its radius from the rotation axis. Data is plotted for 300 μm, 450 μm and 600 μm pitch and for 2 mm, 10 mm and 20 mm field width. The linear component of the spiral motion is 0.1 mm s^{-1} for all cases, which keeps the target dose constant. To increase the beam pitch, the angular velocity must be reduced, resulting in higher exposure times for larger pitches.

The valley dose can be successfully lowered and the valley region widened by increasing the beam pitch for spiralMRT, as seen in figure 9. However, the linear component of the motion introduces an increased microbeam spread resulting in wider beams. The beam pitch is likely to be limited by this effect in order to keep microbeams spatially confined.

The normal tissue sparing of microfractionated radiation fields offers new opportunities to deliver safely high amounts of dose in one single temporal fraction, which is associated with an increased risk of developing negative normal tissue side effects in conventional brain metastases treatment (Minniti *et al* 2016). With the normal tissue sparing capability of spiralMRT, the tolerance of single fraction RT could be increased, it would reduce the treatment time for palliative treatment by moving from multiple fractions to one fraction and it may even offer new opportunities for curative approaches.

7. Conclusion

The spatial fractionation of the entrance beams in spiralMRT can help sparing normal tissue when compared to tomotherapy. It has been shown that valley doses are 40% lower than corresponding tomotherapy doses (see figures 9 (e) and (f)), while a homogeneous dose can be maintained in the target region.

The beam width is affected by the linear component of the helical motion, but nominally 50 μm wide beams do not exceed 100 μm effective beam width, when a pitch of 450 μm or lower is applied. Beams exceeding this threshold are associated with a rapidly decreasing normal tissue recovery (Serduc *et al* 2014).

Necessary dose rates will be substantially higher than in conventional RT, but by two orders of magnitude lower than currently employed dose rates at synchrotron sources used for MRT (100 Gy s^{-1} instead of 10 kGy s^{-1}). The associated risk of over-dosage when handling such high dose rates is reduced accordingly.

The increased photon absorption in the bone region is a common disadvantage of spiralMRT and interlaced MRT, when confronted with conventional megavoltage RT, which leads to an increased dose deposition and might locally impair positive effects.

This physical evaluation of the potential of spiralMRT overall comes to a positive conclusion, the next step should be biological experiments on the anticipated benefits to healthy tissue.

8. Outlook

This publication introduces the basic idea of spiralMRT and highlights certain parameters. Many more optimisations could be done, improving the quality of a spiralMRT treatment, such as introducing intensity modulation to spare organs at risk in the beam path and to ensure a homogeneous irradiation of non-centrally located targets. Conformal irradiation would reduce the valley dose that is correlated with the total beam cross section (Martínez-Rovira *et al* 2012). The dependence of the setup on angular misalignment of the primary microbeam and the rotation axis, as well as the technical feasibility with currently available equipment are further points to be investigated.

Compact radiation sources reaching sufficient dose rates are probably available in the mid-term future with a suitable x-ray energy spectrum. Inverse Compton scattering sources (Jacquet 2014) are currently under devel-

opment at different sites and are expected to produce 10^{13} photons per second (Jacquet and Suortti 2015). Distributed over a 20 mm × 20 mm reference field, this flux corresponds to an approximate dose rate of 1 Gy s^{-1} in 20 mm depth in water for 100 keV photons. Taking into account that the actually used field in this case is only 50 μm high, an appropriate focusing of the photon flux to the aperture will easily lead to an increase of the dose rate by a factor of 10 or more. Thus, the technical demands on the radiation flux for spiralMRT may be met in the future by inverse Compton scattering sources.

Another yet theoretical concept are line-focus x-ray tubes (Bartzsch and Oelfke 2017) which may deliver dose rates in the order of 100 Gy s^{-1} and radiation fields with centimetre-sized diameter.

The beam divergence is an important factor when it comes to novel radiation sources. It may broaden the spiralMRT exit beam, while the entrance beam would profit from a better focusing. As soon as the specifications of candidate sources are known, an investigation of the effect should take place. However, the ThomX inverse Compton source is expected to deliver radiation within a 1.5 mrad cone (half opening) (Jacquet and Suortti 2015), i.e. 30 mm beam diameter at 10 m distance from the source.

Acknowledgments

The authors thank Audrey Bouchet, Tomasz Wysokinski, Jean Laissue, and Stefan Bartzsch for their comments on this research project. The Agence Nationale de la Recherche is acknowledged for financial support under grant no. ANR-13-BSV1-0012, as well as the COST action TD1205 'Innovative Methods in Radiotherapy and Radiosurgery using Synchrotron Radiation'.

ORCID iDs

Mattia Donzelli https://orcid.org/0000-0002-1881-4331

References

Agostinelli S *et al* 2003 Geant4a simulation toolkit *Nucl. Instrum. Methods Phys. Res.* A **506** 250–303
Allison J *et al* 2006 Geant4 developments and applications *IEEE Trans. Nucl. Sci.* **53** 270–8
Bartzsch S and Oelfke U 2017 Line focus x-ray tubes—a new concept to produce high brilliance x-rays *Phys. Med. Biol.* **62** 8600
Bouchet A, Bräuer-Krisch E, Prezado Y, El Atifi M, Rogalev L, Le Clech C, Laissue J A, Pelletier L and Le Duc G 2016 Better efficacy of synchrotron spatially micro-fractionated radiotherapy than uniform radiotherapy on glioma *Int. J. Radiat. Oncol. Biol. Phys.* **95** 1485–94
Bouchet A *et al* 2010 Preferential effect of synchrotron microbeam radiation therapy on intracerebral 9L gliosarcoma vascular networks *Int. J. Radiat. Oncol. Biol. Phys.* **78** 1503–12
Bräuer-Krisch E, Serduc R, Siegbahn E A, Le Duc G, Prezado Y, Bravin A, Blattmann H and Laissue J A 2010 Effects of pulsed, spatially fractionated, microscopic synchrotron x-ray beams on normal and tumoral brain tissue *Mutat. Res.* **704** 160–6
Crosbie J C, Fournier P, Bartzsch S, Donzelli M, Cornelius I, Stevenson A W, Requardt H and Braeuer-Krisch E 2015 Energy spectra considerations for synchrotron radiotherapy trials on the ID17 bio-medical beamline at the european synchrotron radiation facility *J. Synchrotron Radiat.* **22** 1035–41
Dilmanian F A *et al* 2002 Response of rat intracranial 9L gliosarcoma to microbeam radiation therapy *Neuro-oncol.* **4** 26–38
Dilmanian F A, Zhong Z, Bacarian T, Benveniste H, Romanelli P, Wang R, Welwart J, Yuasa T, Rosen E M and Anschel D J 2006 Interlaced x-ray microplanar beams: a radiosurgery approach with clinical potential *Proc. Natl Acad. Sci.* **103** 9709–14
Fournier P, Crosbie J C, Cornelius I, Berkvens P, Donzelli M, Clavel A, Rosenfeld A B, Petasecca M, Lerch M L F and Bräuer-Krisch E 2016 Absorbed dose-to-water protocol applied to synchrotron-generated x-rays at very high dose rates *Phys. Med. Biol.* **61** N349
Jacquet M 2014 High intensity compact compton x-ray sources: challenges and potential of applications *Nucl. Instrum. Methods Phys. Res.* B **331** 1–5
Jacquet M and Suortti P 2015 Radiation therapy at compact compton sources *Phys. Medica* **31** 596–600
Laissue J A, Blattmann H and Slatkin D N 2012 Alban kohler (1874–1947): inventor of grid therapy *Z. Med. Phys.* **22** 90–9
Laissue J A *et al* 2001 The weanling piglet cerebellum: a surrogate for tolerance to MRT (microbeam radiation therapy) in pediatric neuro-oncology *Proc. SPIE* **4508** 65–73
Laissue J A *et al* 1998 Neuropathology of ablation of rat gliosarcomas and contiguous brain tissues using a microplanar beam of synchrotron-wiggler-generated x rays *Int. J. Cancer* **78** 654–60
Livingstone J, Stevenson A W, Butler D J, Häusermann D and Adam J F 2016 Characterization of a synthetic single crystal diamond detector for dosimetry in spatially fractionated synchrotron x-ray fields *Med. Phys.* **43** 4283–93
Martínez-Rovira I, Sempau J and Prezado Y 2012 Development and commissioning of a Monte Carlo photon beam model for the forthcoming clinical trials in microbeam radiation therapy *Med. Phys.* **39** 119–31
Minniti G, Scaringi C, Paolini S, Lanzetta G, Romano A, Cicone F, Osti M, Enrici R M and Esposito V 2016 Single-fraction versus multifraction (3 × 9 Gy) stereotactic radiosurgery for large (>2 cm) brain metastases: a comparative analysis of local control and risk of radiation-induced brain necrosis *Int. J. Radiat. Oncol. Biol. Phys.* **95** 1142–8
Pouyatos B *et al* 2016 Synchrotron x-ray microtransections: a non invasive approach for epileptic seizures arising from eloquent cortical areas *Sci. Rep.* **6** 27250
Renier M 2016 personal communication
Romanelli P, Striano P, Barbarisi M, Coppola G and Anschel D J 2012 Non-resective surgery and radiosurgery for treatment of drug-resistant epilepsy *Epilepsy Res.* **99** 193–201

Serduc R, Bouchet A, Pouyatos B, Renaud L, Bräuer-Krisch E, Le Duc G, Laissue J A, Bartzsch S, Coquery N and Van de Looij Y 2014 Synchrotron x ray induced axonal transections in the brain of rats assessed by high-field diffusion tensor imaging tractography *PLoS One* **9** e88244

Serduc R *et al* 2010 High-precision radiosurgical dose delivery by interlaced microbeam arrays of high-flux low-energy synchrotron x-rays *PLoS One* **5** e9028

Serduc R *et al* 2006 *In vivo* two-photon microscopy study of short-term effects of microbeam irradiation on normal mouse brain microvasculature *Int. J. Radiat. Oncol. Biol. Phys.* **64** 1519–27

Shinohara K, Kondoh T, Nariyama N, Fujita H, Washio M and Aoki Y 2014 Optimization of x-ray microplanar beam radiation therapy for deep-seated tumors by a simulation study *J. X-Ray Sci. Technol.* **22** 395–406

Smyth L M, Senthi S, Crosbie J C and Rogers P A 2016 The normal tissue effects of microbeam radiotherapy: What do we know, and what do we need to know to plan a human clinical trial? *Int. J. Radiat. Biol.* **92** 302–11

Spiga J, Siegbahn E, Bräuer-Krisch E, Randaccio P and Bravin A 2007 The geant4 toolkit for microdosimetry calculations: application to microbeam radiation therapy (MRT) *Med. Phys.* **34** 4322–30

Studer F, Serduc R, Pouyatos B, Chabrol T, Bräuer-Krisch E, Donzelli M, Nemoz C, Laissue J, Estève F and Depaulis A 2015 Synchrotron x-ray microbeams: a promising tool for drug-resistant epilepsy treatment *Phys. Med.* **31** 607–14